NEUROSCIENCE

Layer-specific pain relief pathways originating from primary motor cortex

Zheng Gan[1], Vijayan Gangadharan[1]†, Sheng Liu[1], Christoph Körber[2], Linette Liqi Tan[1], Han Li[1], Manfred Josef Oswald[1], Juhyun Kang[1], Jesus Martin-Cortecero[3], Deepitha Männich[1], Alexander Groh[3], Thomas Kuner[2], Sebastian Wieland[2,4], Rohini Kuner[1]*

The primary motor cortex (M1) is involved in the control of voluntary movements and is extensively mapped in this capacity. Although the M1 is implicated in modulation of pain, the underlying circuitry and causal underpinnings remain elusive. We unexpectedly unraveled a connection from the M1 to the nucleus accumbens reward circuitry through a M1 layer 6-mediodorsal thalamus pathway, which specifically suppresses negative emotional valence and associated coping behaviors in neuropathic pain. By contrast, layer 5 M1 neurons connect with specific cell populations in zona incerta and periaqueductal gray to suppress sensory hypersensitivity without altering pain affect. Thus, the M1 employs distinct, layer-specific pathways to attune sensory and aversive-emotional components of neuropathic pain, which can be exploited for purposes of pain relief.

The primary motor cortex (M1) controls voluntary motor behaviors and has been extensively studied with respect to the physiological processes and neuronal circuitry underlying initiation of movement (*1*). Unexpectedly, the percept of pain also evokes responses in the human primary motor cortex in intracortical recordings and functional neuroimaging studies (*2*). The M1 undergoes plasticity in chronic pain (*3*) and interactions between pain and motor functions are exploited in exercise therapies. However, very little is known about the neurobiological basis for this putative, unconventional role for the M1 in modulating pain perception. Neurostimulation therapies involving transcranial magnetic stimulation or transcranial direct current stimulation (tDCS) over primary motor areas are emerging as attractive alternatives to drug therapy (*4*). However, these are limited in clinical utility by high variability in efficacy, which has been ascribed to a fundamental lack of understanding of the underlying circuitry (*5*, *6*). As observed in human studies, application of anodal tDCS over the M1 alleviates neuropathic hypersensitivity in mice (fig. S1, A and B) (*7*), but does so in a broad manner because diverse adjoining sensory and prefrontal cortical areas that are implicated in pain are also vividly coactivated (fig. S1C).

With the goal of specifically dissecting the role of the M1 in pain relief and elucidating its neurobiological underpinnings, we employed layer- and cell type–specific optogenetic (*8*) and chemogenetic approaches (*9*) for temporally controlled and reversible manipulation of M1 microcircuitry. In mice virally expressing either the excitatory chemogenetic Designer Receptor Exclusively Activated by Designer Drugs (DREADD) hM3Dq (Gq) or mCherry (as control), the DREADD-stimulating ligand Clozapine-N-oxide (CNO) (*9*) was applied before or after induction of neuropathic pain in the spared nerve injury (SNI) model (*10*) (Fig. 1A and fig. S2A; validation and specificity of M1 activation shown in Fig. 1B and fig. S2B). Spatially restricted activation of the M1 hindlimb cortex across all cellular layers, driving hM3Dq expression from the murine synapsin promoter, significantly suppressed peak nociceptive hypersensitivity toward non-noxious mechanical stimulation (0.07 to 0.6 g; mechanical allodynia; Fig. 1C), whereas similar manipulations in non-neuropathic mice led to no changes in nociception (fig. S2C, left panel). Chemogenetically stimulating M1 excitatory neurons specifically, using the murine Camkllα promoter (validation of specificity and efficacy shown in fig. S2, D and E, respectively), recapitulated the specific and beneficial effects on mechanical allodynia and alleviated hypersensitivity toward 5°C cooling, another hallmark of neuropathic pain disorders (*10*) (Fig. 1D and fig. S2F) without affecting motor behaviors (fig. S2, G and H). Suppression of mechanical allodynia was robustly preserved when neuropathic pain was chronically maintained at 8 weeks post-SNI (Fig. 1D). By contrast, chemogenetically stimulating the adjoining somatosensory hindlimb cortex (S1HL) had no impact on neuropathic pain-related behavior (fig. S3A).

Whether M1 stimulation operates through modulation of excitatory or inhibitory neurons has been a topic of much debate (*11*). Signal processing and output of cortical microcircuits is determined by the interplay between excitatory pyramidal neurons and diverse classes of GABAergic interneurons. Parvalbumin-expressing neurons (PV), the largest class of neocortical GABAergic neurons, inhibit deep pyramidal cell layers at the soma, while their distal dendrites are inhibited by Somatostatin-type (SOM) GABAergic neurons that also limit the activity of PV neurons (*12*). Using cell type–specific transgenic mouse lines, we observed that chemogenetic activation of PV neurons in the M1 markedly exacerbated neuropathic hypersensitivity (Fig. 1E and fig. S3, B and C), whereas chemogenetically activating SOM neurons significantly reduced mechanical allodynia (Fig. 1E and fig. S3, B and D). Because DREADD-based cortical activation spans several hours at a time and could thus potentially lead to widespread downstream changes, we also performed temporally restricted optogenetic manipulations using Camkllα promoter–driven expression of Channelrhodopsin (ChR2) (Fig. 1F). Blue light–induced activation of excitatory M1 neurons precisely coinciding with the time frame of sensory stimulation acutely suppressed both mechanical and cold allodynia in neuropathic mice (Fig. 1F and fig. S4A). Temporally limited optogenetic activation of the M1 also enabled us to conduct experiments in a real time paradigm in which different operant chambers with contextual cues were longitudinally paired with either M1 or sham stimulation (fig. S4B). Neuropathic—but not naïve—mice showed real-time conditioned place preference (CPP) for the chamber paired with M1 stimulation (Fig. 1F, bottom panels). Locomotion was not hampered by M1-specific manipulations (fig. S3C).

Which M1 cortical layers deliver the required excitatory output? By employing transgenic mice for layer-specific chemogenetic manipulations, we observed that selective activation of neither layer 2/3 (Fig. 1G and fig. S4D) or layer 6 (Fig. 1H and fig. S4E) influenced nociceptive behaviors in neuropathic mice. By contrast, selectively activating M1 layer 5 recapitulated the anti-hyperalgesic effects seen with whole M1 activation (Fig. 1I and fig. S4F). No sex differences were observed with anti-hyperalgesic effects of activation of M1 or of the individual layers or downstream pathways.

We studied acute changes in expression of the activity marker Fos in neuropathic mice upon chemogenetic activation of M1 excitatory neurons (fig. S5A) and matched this information to the known salient projections of the M1 (*13*, *14*). Amongst the 15 pain-related target regions analyzed, the periaqueductal gray (PAG) and the zona incerta (ZI) stood out. Although the midcingulate and prelimbic cortices also showed changes in Fos, we observed

[1]Pharmacology Institute, Medical Faculty Heidelberg, Heidelberg University, Heidelberg, Germany. [2]Department of Functional Neuroanatomy, Institute for Anatomy and Cell Biology, Medical Faculty Heidelberg, Heidelberg University, Heidelberg, Germany. [3]Institute for Physiology and Pathophysiology, Medical Faculty Heidelberg, Heidelberg University, Heidelberg, Germany. [4]Department of General Internal Medicine and Psychosomatics, Medical Faculty Heidelberg and University Clinic Heidelberg, Heidelberg, Germany.
***Corresponding author. Email: rohini.kuner@pharma.uni-heidelberg.de** †Present address: Institute for Vascular and Islet Cell Biology, German Diabetes Center, Leibniz Center for Diabetes Research at Heinrich Heine University Düsseldorf, Düsseldorf, Germany.

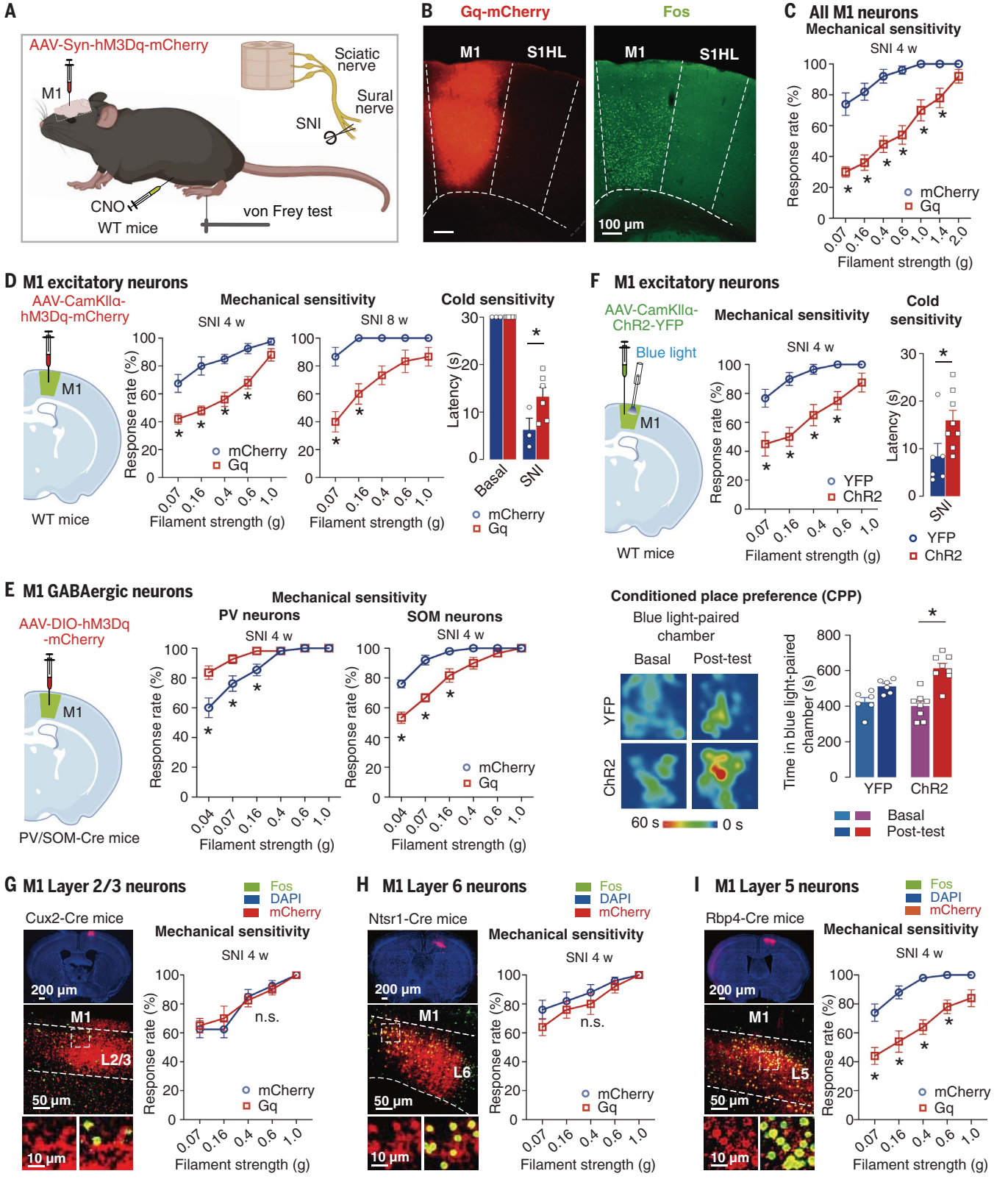

Fig. 1. M1-restricted activation leads to pain relief in neuropathic mice and reversal of allodynia occurs through layer 5. (**A**) Chemogenetic activation strategy for the M1 cortex through hM3Dq (Gq) expression and Clozapine-N-oxide (CNO) application with spared nerve injury (SNI). (**B**) M1 chemogenetic targeting (left) and activation (right; anti-Fos immunohistochemistry). S1HL, primary somatosensory hindlimb cortex. (**C**) Mechanical hypersensitivity to von Frey filament force at 4 weeks (4 w) post-SNI (n = 10 mice per group) in CNO-treated Gq- or mCherry-injected mice (control). (**D**) Chemogenetic activation strategy for M1 excitatory neurons (left) and reversal of mechanical allodynia (middle) (at SNI 4 w, mCherry: n = 8, Gq: n = 10 mice; at SNI 8 w: n = mCherry: n = 3, Gq: n = 6 mice) and cold allodynia (mCherry: n = 3, Gq: n = 6 mice, F = 1.268, P = 0.0362). (**E**) Chemogenetic activation strategy for M1 GABAergic populations

(left) and effect on mechanical allodynia (right) upon activation of PV neurons (n = 11 mice per group) or SOM neurons (mCherry: n = 10, Gq: n = 12 mice). (**F**) Optogenetic activation strategy for M1 excitatory neurons (left), reversal of mechanical allodynia (top middle; YFP: n = 6, ChR2: n = 6 mice) and cold allodynia (top right; n = 8 mice per group); CPP to a chamber paired with optogenetic stimulation (bottom), shown as heat plots (bottom left, below) and cumulative time (bottom right; YFP: n = 6, ChR2: n = 8 mice). (**G**, **H**, and **I**) Layer-specific chemogenetic M1 activation using transgenic mice targeting layer 2/3 [(G) Cux2-Cre, n = 8 mice per group], layer 6 [(H) Ntsr1-Cre, n = 10 mice per group), and layer 5 [(I) Rbp4-Cre, n = 10 mice per group], expression areas [(left panels in (G) to (I)] and mechanical allodynia [(right panels in (G) to (I)]; $P < 0.05$ for Gq curves for layer 5 versus layer 2/3 and layer 6. Analysis of variance (ANOVA) for random measures followed by post-hoc Sidak's test. * represents $P < 0.05$; exact F and P values for all groups are given in table S1. Data are shown as mean ± standard error of the mean (SEM).

in anterograde viral tracing experiments that they do not receive direct projections from the M1 (fig. S5B), suggesting indirect downstream modulation. We therefore first expressed ChR2 in all excitatory neurons of the hindlimb M1 cortex and optogenetically stimulated M1 projections to the ZI (electrophysiological validation in Fig. 2A and fig. S6, A and B) or the lateral and ventrolateral PAG (lPAG/vlPAG, electrophysiological validation in Fig. 2B and fig. S6, C and D), and observed that each can significantly—but only partly—suppress neuropathic allodynia. Moreover, each was weaker than stimulation of either the whole M1 or layer 5 alone, suggesting that these two pathways act independently and additively. The ZI is a subthalamic nucleus that receives dense nociceptive input through the spinothalamic tract (*15*). However, very little is known about the underlying cellular circuitry and modulation of the ZI by the M1 remains largely unexplored. ZI neurons are not homogenous in function but show a high level of specificity in modulating defensive behaviors, binge eating, hunting, and sleep, depending upon their neurochemical identity and subdivision into distinct anatomical sectors (*16*, *17*). We observed that hindlimb M1 neurons project to the dorsal (ZId) and ventral (ZIv) sectors (Fig. 2A), but not to the rostral and caudal sectors. Tracing analyses using layer-specific transgenic mice revealed that hindlimb M1 layer 5 but not layer 6 neurons project to the ZI (fig. S7, A and B), consistent with dye labeling analyses in vibrissae M1 (*17*). Keeping tracer bias and limitations related to viral tropism in mind, we performed retrograde labeling with Fluorogold (fig. S7B) or retrograde AAV-YFP virus (Fig. 2C) injected in the ZI and found labeled layer 5, but not layer 6, neurons in the M1. The dorsal sector of the ZI predominantly harbors excitatory neurons, e.g., nNos-expressing neurons, that send excitatory projections to the midbrain and brainstem nuclei, such as the PAG and raphe nuclei, which gate the modulation of pain. By contrast, ZIv is overwhelmingly GABAergic in nature, including PV, SOM, and Tac1 subclasses, and exerts feedforward inhibition in projection areas, particularly the thalamus (*15*, *18*). A number of our observations collectively revealed that M1 activation preferentially fosters output of the ZI to the midbrain and brainstem. First, employing a viral strategy that specifically enables trans-synaptic labeling of projection targets with a fluorescent reporter (validated in fig. S8A) in combination with viral labeling of GABAergic neurons (Fig. 2D), we observed that most ZI neurons receiving M1 monosynaptic inputs comprise non-GABAergic neurons. Coimmunohistochemistry with marker proteins for the PV, SOM, and Tac1 populations further revealed that most of the neurons receiving M1 inputs in the ZId and ZIv, respectively, do not belong to the aforementioned GABAergic neuron categories (Fig. 2E). Second, optogenetic M1 stimulation in mice with SNI increased the activity marker Fos in neurons of the ZId but not in the ZIv, and this increase was specific to non-GABAergic neurons (Fig. 2F). GABAergic neurons overall—particularly the PV-type GABAergic neurons—showed a decrease in Fos expression upon M1 stimulation post-SNI (Fig. 2G), suggesting modulation within local ZI microcircuits.

The PAG has been linked with motor cortex stimulation–induced analgesia (*6*). However, neither causality nor cellular connectivity has been addressed. We observed that the hindlimb M1 neurons project densely to the upper segment of the ventrolateral column (vlPAG) and the lower segment of the lateral column (lPAG) (Fig. 2B), but not the dorsal and medial columns of the PAG. Retrograde labeling from the lPAG and vlPAG using viral transfer- or Flurogold-labeled M1 neurons (Fig. 2H and fig. S8B, respectively) only in layer 5 and not layer 6, which was further validated through anterograde viral tracing in layer-specific transgenic mice (fig. S7A). Optogenetically activating projections of layer 5 M1 neurons to the lPAG and vlPAG robustly attenuated mechanical allodynia in neuropathic mice (Fig. 2I and fig. S9A). Optogenetic stimulation of the M1 layer 5-PAG pathway increased Fos expression significantly in both GABAergic neurons (fig. S9B) and non-GABAergic neurons (Fig. 2J) of the lPAG-vlPAG. Trans-synaptic labeling (see Fig. 2D) revealed that more than 80% of the lPAG-vlPAG neurons receiving direct synaptic inputs from the M1 are non-GABAergic in nature in SNI mice (Fig. 2K). In the vlPAG, chemogenetic activation of excitatory neurons inhibits nociception, whereas activation of GABAergic neurons facilitates nociception (*19*). Our data thus suggest that M1 layer 5 activation shifts the neuronal excitation-inhibition balance in the vlPAG toward increased activation. Optogenetic activation of the M1 layer 5-PAG pathway or the M1 layer 5-ZI pathway did not affect motor behaviors in neuropathic or uninjured mice (fig. S9, C to E, and movies S1 to S3) or elicit CPP in uninjured mice (fig. S9G). Retrograde viral labeling with dual constructs revealed that most M1 projections to the ZI and vlPAG are collaterals (fig. S10A) and transsynaptic anterograde tracing showed that both lPAG/vlPAG neurons and ZI neurons that receive M1 inputs project to areas such as the locus coeruleus (LC) and rostral ventromedial medulla (RVM) that are involved in descending modulation of spinal nociception, in addition to diverse other functions (fig. S10, B and C). It has been proposed that the PAG-RVM pathway enhances descending inhibition of nociception, whereas PAG neurons projecting to the locus ceruleus—which can be specifically identified through expression of the signaling enzyme PLCβ4—suppress descending analgesic pathways (*20*) (Fig. 2L, left panel). Although PLCβ4-expressing neurons were abundant in lPAG-vlPAG, they constituted less than 10% of neurons that were trans-synaptically labeled from incoming M1-PAG projections (Fig. 2L, middle and right panels). Furthermore, whereas optogenetic M1 stimulation in neuropathic mice led to a significant increase in Fos expression in PAG neurons receiving direct synaptic inputs from the M1 (Fig. 2J), the proportion of PLCβ4-expressing neurons showing Fos expression decreased significantly (Fig. 2M).

How does M1 activation reduce negative emotional valence in neuropathic pain? Optogenetic activation of the M1-ZI, M1-PAG, or M1 layer 5-PAG pathways did not reproduce the CPP phenotype (Fig. 3A) displayed by neuropathic mice with optogenetic stimulation of the entire hindlimb M1 (see Fig. 1F). Layer 6 of the M1 densely projects to diverse thalamic nuclei (*13*), and the mediodorsal thalamus (MD) is an important station that relays ascending sensory inputs related to the aversive component of pain to prefrontal and limbic cortices (*21*). We therefore studied M1 connectivity with the MD in detail using anterograde (Fig. 3B and fig. S11A) viral tracing experiments and noted that layer 6 of hindlimb M1 predominantly targets the lateral domain of the MD (MD_L). By contrast, the MD_L does not receive inputs from

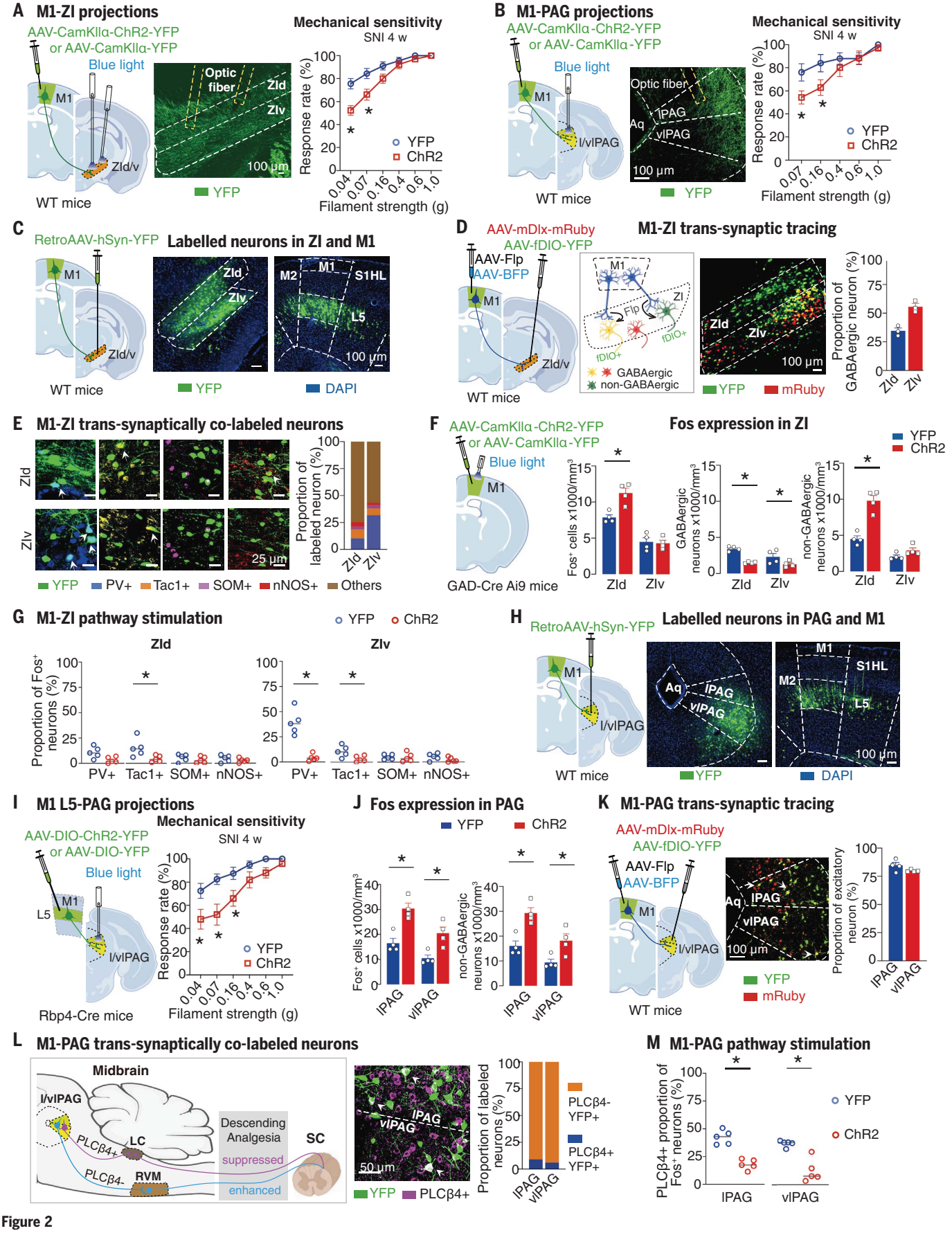
A M1-ZI projections
AAV-CamKIIα-ChR2-YFP
or AAV-CamKIIα-YFP
Blue light
M1
Zld/v
WT mice
Optic fiber
Zld
Zlv
100 μm
YFP
Mechanical sensitivity
SNI 4 w
Response rate (%)
YFP
ChR2
Filament strength (g)
B M1-PAG projections
AAV-CamKIIα-ChR2-YFP
or AAV-CamKIIα-YFP
Blue light
M1
l/vlPAG
WT mice
Optic fiber
Aq
lPAG
vlPAG
100 μm
YFP
Mechanical sensitivity
SNI 4 w
Response rate (%)
YFP
ChR2
Filament strength (g)
C
RetroAAV-hSyn-YFP
Labelled neurons in ZI and M1
M1
Zld/v
WT mice
Zld
Zlv
YFP
M2
M1
S1HL
L5
100 μm
DAPI
D
AAV-mDlx-mRuby
AAV-fDIO-YFP
AAV-Flp
AAV-BFP
M1
Zld/v
WT mice
M1
ZI
Flp
fDIO+
fDIO+
GABAergic
non-GABAergic
M1-ZI trans-synaptic tracing
Zld
Zlv
100 μm
YFP
mRuby
Proportion of GABAergic neuron (%)
Zld
Zlv
E M1-ZI trans-synaptically co-labeled neurons
Zld
Zlv
25 μm
Proportion of labeled neuron (%)
Zld
Zlv
YFP
PV+
Tac1+
SOM+
nNOS+
Others
F
AAV-CamKIIα-ChR2-YFP
or AAV-CamKIIα-YFP
Blue light
M1
GAD-Cre Ai9 mice
Fos expression in ZI
YFP
ChR2
Fos+ cells x1000/mm3
GABAergic neurons x1000/mm3
non-GABAergic neurons x1000/mm3
Zld
Zlv
G M1-ZI pathway stimulation
YFP
ChR2
Zld
Zlv
Proportion of Fos+ neurons (%)
PV+
Tac1+
SOM+
nNOS+
H
RetroAAV-hSyn-YFP
Labelled neurons in PAG and M1
M1
l/vlPAG
WT mice
Aq
lPAG
vlPAG
M1
S1HL
M2
L5
100 μm
YFP
DAPI
I M1 L5-PAG projections
AAV-DIO-ChR2-YFP
or AAV-DIO-YFP
Blue light
M1
L5
l/vlPAG
Rbp4-Cre mice
Mechanical sensitivity
SNI 4 w
Response rate (%)
YFP
ChR2
Filament strength (g)
J Fos expression in PAG
YFP
ChR2
Fos+ cells x1000/mm3
non-GABAergic neurons x1000/mm3
lPAG
vlPAG
K M1-PAG trans-synaptic tracing
AAV-mDlx-mRuby
AAV-fDIO-YFP
AAV-Flp
AAV-BFP
M1
l/vlPAG
WT mice
Aq
lPAG
vlPAG
100 μm
YFP
mRuby
Proportion of excitatory neuron (%)
lPAG
vlPAG
L M1-PAG trans-synaptically co-labeled neurons
Midbrain
l/vlPAG
PLCβ4+
LC
PLCβ4-
RVM
Descending Analgesia
suppressed
enhanced
SC
lPAG
vlPAG
50 μm
YFP
PLCβ4+
Proportion of labeled neurons (%)
PLCβ4- YFP+
PLCβ4+ YFP+
lPAG
vlPAG
M M1-PAG pathway stimulation
PLCβ4+ proportion of Fos+ neurons (%)
YFP
ChR2
lPAG
vlPAG

Figure 2

Fig. 2. M1 layer 5 projections to specific neuronal populations in the ZI and PAG inhibit neuropathic mechanical allodynia. (**A** and **B**) Optogenetic stimulation of M1 excitatory neuron projections to ZI dorsal (ZId) and ventral (ZIv) domains (A) or to PAG lateral (lPAG) and ventrolateral (vlPAG) columns (B). Shown are schematics (left panels), labeled projections (middle panels), and impact on mechanical allodynia (right panels) for the ZI [(A) YFP: n = 9, ChR2: n = 13 mice] and PAG [(B) YFP: n = 5, ChR2: n = 7 mice]. (**C**) Strategy (left) for retrograde labeling of M1 layer 5 neurons (right) after injection in ZI (middle). (**D**) Strategy (left) for viral trans-synaptic YFP labeling of ZI neurons receiving M1 afferent projections (middle) and analysis of non-GABAergic neurons [(right) (n = 3 mice per group)]. (**E**) Immunohistochemical characterization of trans-synaptically YFP-labeled ZI neurons receiving M1 afferent inputs (n = 3 mice per group). (**F**) Fos expression in GABAergic neuron reporter mice in ZI domains (right) upon optogenetic activation of M1 excitatory neurons [(left) (n = 3 mice per group]. (**G**) Fos expression upon optogenetic stimulation of the M1-ZI projections (n = 3 to 4 mice per group). (**H**) Strategy [left for labeling of M1 layer 5 neurons (example on right)] retrogradely after viral injection in lPAG/vlPAG (example in middle). (**I** and **J**) Strategy [(I) (left)] for optogenetic stimulation of excitatory M1-lPAG/vlPAG projections and impact on mechanical allodynia [(I), right; YFP: n = 10, ChR2: n = 8 mice] and on Fos expression in lPAG/vlPAG [(J) n = 3 mice per group]. (**K**) Strategy [(left) viral trans-synaptic YFP labeling of PAG neurons receiving M1 afferent projections (middle) and proportion of non-GABAergic neurons (right)] (n = 4 mice per group). (**L** and **M**) Further characterization of trans-synaptically labeled PAG neuron populations receiving M1 afferent input using anti-PLCβ4 immunohistochemistry [(L) n = 3 mice per group] and Fos expression upon optogenetic stimulation of the M1-PAG pathway [(right) n = 3 mice per group]. In statistical analyses for [(A), (B), and (I)]: ANOVA for random measures followed by post-hoc Sidak's test was performed, for [(F), (G), (J), and (M)]: a two-tailed unpaired t test was performed. * represents $P < 0.05$.

layer 5 of the M1 (fig. S11B). Upon expressing ChR2 in either the entire hindlimb M1 (Fig. 3C and fig. S11C) or selectively in layer 6 using a specific transgenic mouse line (Fig. 3D) and optogenetically activating projections specifically in the MD_L (electrophysiological validation in fig. S11D), neuropathic mice developed significant CPP without any change in sensory hypersensitivity (Fig. 3, C and D, and fig. S11, E and F).

Given that the rostral anterior cingulate cortex (rACC) plays a role in the aversive component of pain (*21*), it was reasonable to expect that the layer 6-MD_L pathway targets the rACC to alleviate pain affect in neuropathic mice. However, a number of observations revealed that this is unlikely to be the case. First, dual multisite labeling revealed that the M1 layer 6 projection zone in the MD and the MD domains retrogradely labeled from the rACC do not overlap with each other (Fig. 3E and fig. S12A). Secondly, anterograde labeling revealed that the MD_L domain of the MD makes denser connections with other neocortical domains, such as the M2, as compared with the rACC (fig. S12B). Third, trans-synaptic tracing in mice with virally labeled GABAergic neurons revealed that MD_L neurons receiving direct inputs from M1 layer 6 are almost exclusively non-GABAergic (Fig. 3F); in support, Fos mapping experiments indicated that optogenetic activation of M1 layer 6 enhances activity in non-GABAergic neurons of the MD_L (fig. S12B). However, optogenetic activation of excitatory connectivity from the MD to the rACC evokes aversion (*22*), as opposed to the anti-aversive effects upon activating M1 layer 6-MD connectivity.

We therefore further studied the projections emerging from the MD_L and found sparse termination zones in the prelimbic cortex and the basolateral amygdala (fig. S12C) and dense terminations in the nucleus accumbens (NAc) (Fig. 4A). In Fos labeling experiments, the NAc, but not the prelimbic cortex or basolateral amygdala, demonstrated changes upon optogenetic stimulation of layer 6 M1 neurons (fig. S12D). Thalamic control of the NAc from the paraventricular thalamus represents one of the most salient and functionally well-characterized input pathways into the NAc, which is linked to expression of aversive behaviors (*23*). By contrast, although large scale connectivity analyses on the NAc include inputs from the MD, they have not been functionally interrogated thus far. Our anterograde tracing experiments demonstrated that the MD_L robustly targets the core region of the NAc (NAcC) (Fig. 4A), with sparser connections to the shell (NAcSh) also noted in more medial areas (fig. S12E). More than 90% of NAc neurons are GABAergic medium spiny neurons (MSNs), with a much smaller proportion of local cholinergic interneurons. Using a combination of trans-synaptic viral labeling in transgenic mice with labeling of dopamine receptor D1- or D2-types of GABAergic MSNs using specific transgenic mouse lines (Fig. 4B and fig. S13A), we observed that the MD_L targets both D1- and D2-types of MSNs in the NAc, with a higher density of D2-type MSNs receiving MD_L inputs being observed (Fig. 4B). In patch clamp recordings on MSNs in NAcC, optogenetic terminal stimulation of MD_L-NAcC projections in the NAcC evoked excitatory glutamatergic currents, which are consistent with direct synaptic input (Fig. 4C), thus demonstrating that MD_L-NAcC connections are functional and capable of modulating the activity of NAcC MSNs. In vivo evidence for functionality of this pathway was given by fiber photometry imaging experiments, in which were expressed the genetically encoded calcium indicator GCaMP7.0f in NAc and red-shifted excitatory opsin ChrimsonR in the MD_L (Fig. 4D, left panel). In vivo optogenetic stimulation of MD_L neurons in awake mice induced acute bulk calcium transients in NAc (Fig. 4D, middle panel, and fig. S13B). Upon longitudinal testing, all tested mice demonstrated a trend for decreased bulk calcium transients evoked by MD_L-NAc pathway stimulation 1-week post-SNI, when peak neuropathic pain is established. However, reduction in peak amplitude did not reach statistical significance (Fig. 4D, right panel). Finally, to test the in vivo functional significance of the MD_L-NAc pathway—particularly its relevance to alleviation of neuropathic pain upon M1 activation—we performed behavioral experiments integrating a trans-synaptic optogenetic approach enabling specific activation of terminations in the NAcC of only MD_L neurons receiving direct inputs from the M1 (scheme shown in Fig. 4E, left panel, and fig. S13C). Activating this novel M1-MD_L-NAcC pathway led to CPP in neuropathic mice (Fig. 4E, middle panels), but not in baseline conditions in uninjured mice (fig. S13D), without affecting neuropathic sensory hypersensitivity (Fig. 4E, right panel, and fig. S13E) or motor behaviors (fig. S13, F and G). To consolidate these findings with additional analyses of pain-related negative valence, we performed prolonged application of a strong pinch stimulus in uninjured mice (Fig. 4F) (*24*) and studied coping behaviors comprising attending and escape-related behaviors in video monitoring experiments (movie S4). Chemogenetic activation of whole M1 or optogenetic activation of the M1 pathways to ZI, PAG, or MD_L-NAcC did not alter coping behavior during pinch application (clip on, Fig. 4F, left panel), whereas only activation of the M1-MD_L-NAcC pathway significantly reduced ongoing pain-related coping behaviors persisting after removal of the noxious stimulus (clip off, Fig. 4F, right panel, and movies S5 to S7). In mice with nerve injury, only activation of the M1-MD_L-NAcC significantly reduced cold allodynia-related coping behaviors to a 3°C cold stimulus (Fig. 4G and movies S8 to S10). Analysis of baseline and noxious stimulus–induced Fos expression in conjunction with cell type–selective neuronal markers (*24*, *25*) revealed that neurons involved in ascending relay of noxious information or descending modulation of spinal nociception are differentially affected by activation of the individual M1 pathways projecting to the ZI, PAG, or MD_L-NAcC (see Supplementary note 1 for details; figs. S14 and S15).

These results uncover a notable functional dichotomy of circuit connectivity of layer 5 and

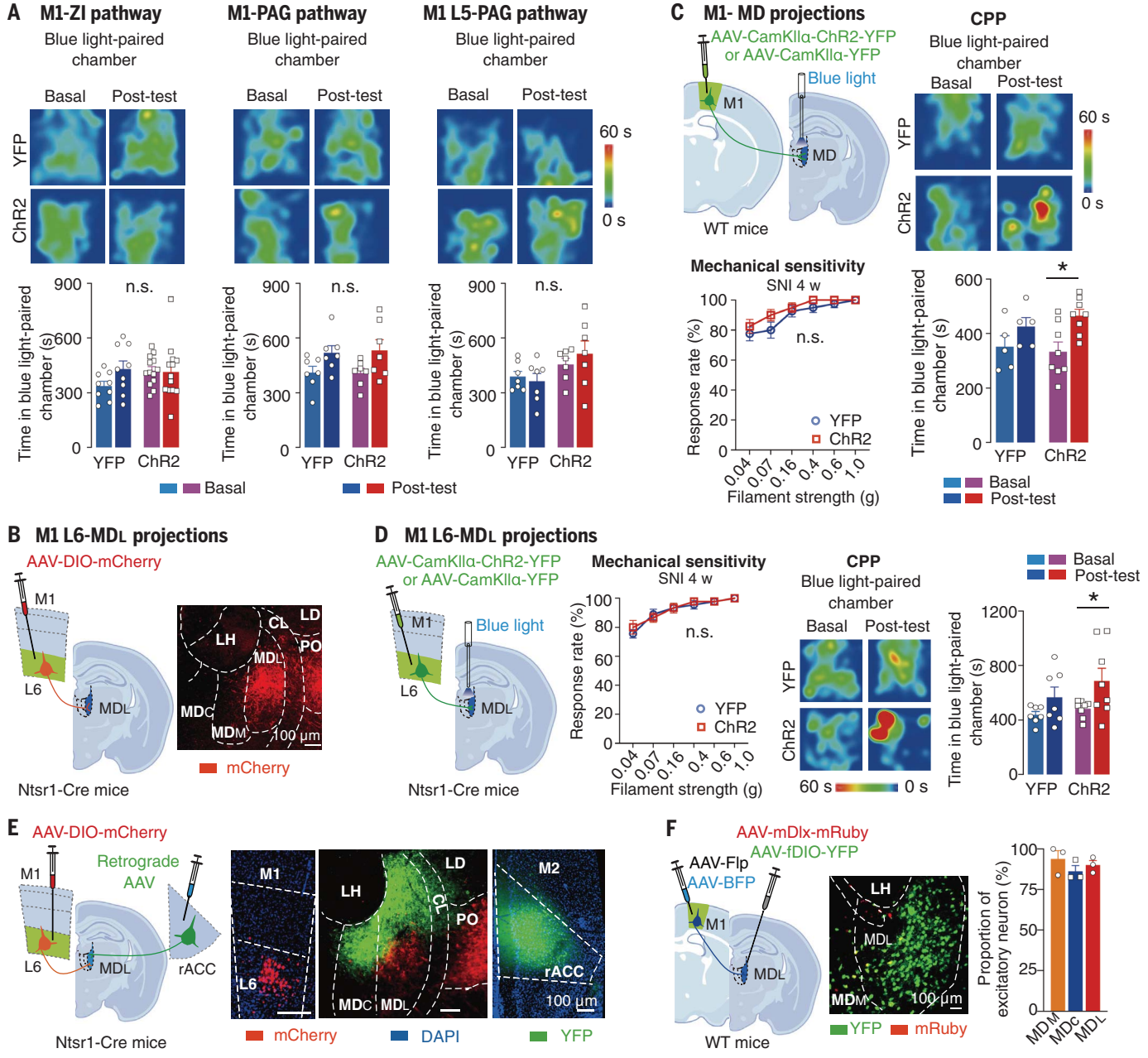

Fig. 3. Activation of M1 layer 6 neurons specifically reduces negative affective valence in neuropathic pain through projections to the mediodorsal thalamus. (**A**) Lack of CPP following optogenetic stimulation of M1-ZI projections, M1-PAG projections, or layer 5 M1-PAG projections. Shown are heat plots of time spent in an optogenetic stimulation-paired chamber (top) and the respective quantitative summary (bottom) [(left) YFP: n = 9, ChR2: n = 13 mice, (middle) n = 9 mice per group, (right) n = 7 mice per group). (**B**) Strategy (left) for viral anterograde tracing of M1 layer 6 projections to the lateral mediodorsal thalamus [MD_L (middle)] using Ntsr1-Cre mice. (**C** and **D**) Impact of optogenetic stimulation of M1 projections to the MD (C) or specifically of M1 layer 6 projections to the MD_L (D) on neuropathic mechanical allodynia (n = 8 to 9 mice per group) and CPP (YFP: n = 5 to 7, ChR2: n = 8 mice). (**E**) Schematic (left) and examples (right) demonstrating lack of convergence within the MD_L (middle) of M1-MD_L afferents labeled anterogradely from M1 layer 6 neurons (red in left image) and efferents from the MD to the rACC labeled retrogradely from the rACC (green in right image) (n = 4 mice). (**F**) Viral trans-synaptic YFP labeling of MD_L neurons receiving M1 afferent projections (middle) and analysis of non-GABAergic neurons [(right) n = 3 mice per group); AAV-BFP was injected as a local targeting control. ANOVA for random measures was performed followed by post-hoc Sidak's test. * represents $P < 0.05$.

layer 6 pyramidal neurons of the hindlimb M1 in regulating two distinct components of pain (fig. S16). The study identifies the ZI as an important target of M1-mediated cortical control of nociceptive hypersensitivity, particularly by strengthening excitatory outputs to the descending nociceptive modulatory centers, such as raphe nuclei and the PAG. Neuropathic pain involves both a depletion of ZI activity (*26*) and a loss of descending bulbospinal inhibitory control of nociception through the PAG. The implication of our findings is that in neuropathic conditions M1 activation can restore balance in the ZI and the PAG through layer 5 pathways and thus

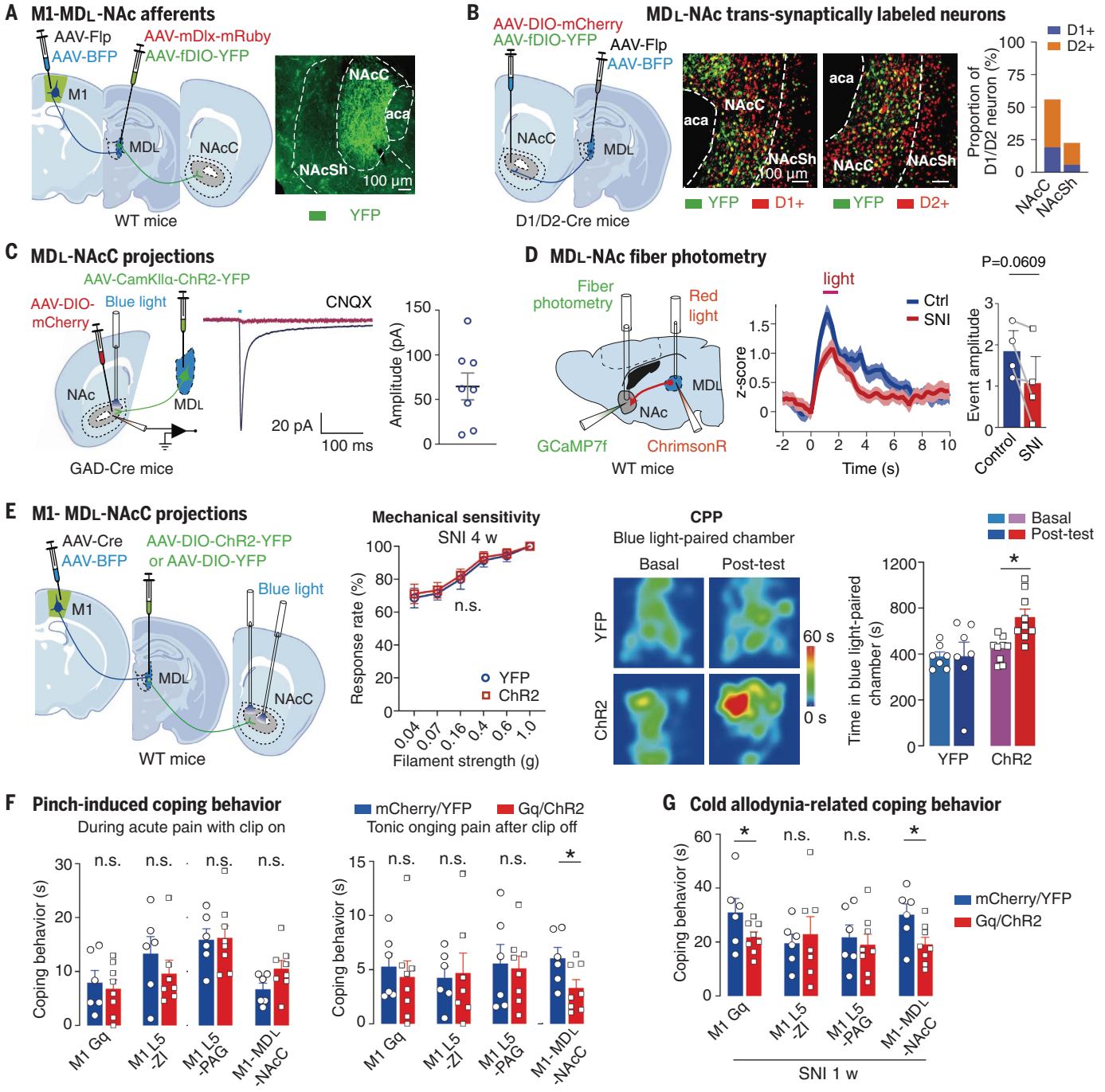

Fig. 4. Unraveling of a functional M1-MD$_L$-nucleus accumbens (NAc) pathway alleviating negative affective valence in neuropathic pain. (**A**) A trans-synaptic viral labeling approach for identifying efferent connections of MD$_L$ neurons receiving direct input from M1 layer 6 neurons (schematic on the left), which reveal the NAc core (NAcC) as a major target and parts of the NAc shell (NAcSh) (example image on right). (**B**) Virally mediated trans-synaptic YFP labeling of neurons in the NAcC and NAcSh receiving afferent projections from the MD$_L$ (left) and their subdivision into D1- and D2-expressing populations using D1-Cre and D2-Cre mice (middle) and quantification [(right) n = 5 sections per group]. (**C**) Patch clamp recordings of activity of NAc GABAergic MSNs in brain slices upon optogenetic stimulation of MD$_L$-NAcC projections with strategy (left), example traces [(middle) blocked by glutamate receptor channel antagonist CNQX] and quantification [(right) n = 8 cells from 3 mice.] (**D**) In vivo fiber photometry recordings of calcium transients through GCaMP7f imaging in the NAc upon ChrimsonR-mediated optogenetic stimulation of MD$_L$-NAc projections longitudinally across baseline (control) and post-SNI conditions with strategy (left), example traces (middle), and quantification [(right) n = 4 mice)]. (**E**) Optogenetic stimulation of MD$_L$-NAcC efferent projections specifically originating from MD$_L$ neurons receiving M1 afferent inputs (left) and impact on mechanical allodynia (n = 7 mice in the YFP group and 9 mice in the ChR2 group) and CPP in neuropathic mice (YFP: n = 7, ChR2: n = 9 mice). AAV-BFP: injection control. (**F** and **G**) Changes in coping behaviors during [(F) left] and after [(F) right] prolonged pinch in uninjured mice and in relation to cold allodynia in neuropathic mice (G) upon chemogenetic M1 activation or optogenetic stimulation of M1 pathways as indicated. In [(E), (F), and (G)], ANOVA for random measures followed by post-hoc Sidak's test was performed; for (D), a one-tailed paired t test was performed. * represents $P < 0.05$.

aid in regaining normal nociceptive sensitivity by controlling both ascending and descending information flow in somatosensory nociceptive pathways (fig. S16). Confounding motor effects upon activation of M1 layer 5-corticospinal projections, which activate spinal motor neurons, are unlikely given lack of changes in motor behaviors in optogenetic/chemogenetic experiments and lack of effect on baseline paw withdrawal in the absence of neuropathy.

The elucidation of a previously unknown M1 layer 6-MD_L-NAcC pathway in this study demonstrates that modulation by the primary motor cortex is not restricted to sensorymotor circuitry controlling spinally mediated nociceptive reflexive behaviors but is also a major regulator of emotional processing. Although the classical view postulates antagonistic roles for D1 and D2 neurons in reward and aversion, more recent studies have revealed a more complex role for both D1 and D2-expressing NAc neurons in motivated behaviors depending upon context, early versus persistent phases, and type or origin of afferent input (*27*, *28*). D2-expressing MSNs undergo long-term depression through depletion of excitatory inputs in neuropathic pain conditions (*29*). There is mounting evidence for depletion of dopamine as well as disbalance between D1- and D2-MSN activity in the NAc in chronic pain states (*30*). Our observation that MD_L neurons receiving excitatory inputs from the M1 can stimulate D1 and D2 neurons through glutamatergic transmission thus opens up the possibility that M1 activation can bypass the accumbal dopamine deficit and restore balance in the dysregulated MSN circuitry in neuropathic pain conditions, a hypothesis which requires detailed testing. Both layer 5- and layer 6-derived pathways to the ZI/PAG or MD_L-NAcC did not impact normal nociception in the absence of injury, suggesting that this level of control specifically emerges in neuropathic pain conditions and will not hamper the protective function of physiological pain. These insights, coupled with our observation that chronically established neuropathic pain can be reversed by activation of layer 5/layer 6-dependent pathways, will help provide insights for developing and improving neurostimulation therapies for optimal pain control.

REFERENCES AND NOTES

1. C. L. Ebbesen, M. Brecht, *Nat. Rev. Neurosci.* **18**, 694–705 (2017).
2. M. Frot, M. Magnin, F. Mauguière, L. Garcia-Larrea, *Hum. Brain Mapp.* **34**, 2655–2668 (2013).
3. R. Peyron *et al*., *Neurology* **63**, 1838–1846 (2004).
4. N. Attal *et al*., *Brain* **144**, 3328–3339 (2021).
5. K. Gatzinsky *et al*., *Scand. J. Pain* **21**, 8–21 (2020).
6. X. Moisset, D. C. de Andrade, D. Bouhassira, *Eur. J. Pain* **20**, 689–700 (2016).
7. Z. Gan, H. Li, P. V. Naser, M. J. Oswald, R. Kuner, *Sci. Rep.* **11**, 9735 (2021).
8. C. K. Kim, A. Adhikari, K. Deisseroth, *Nat. Rev. Neurosci.* **18**, 222–235 (2017).
9. S. M. Sternson, B. L. Roth, *Annu. Rev. Neurosci.* **37**, 387–407 (2014).
10. I. Decosterd, C. J. Woolf, *Pain* **87**, 149–158 (2000).
11. J. P. Nguyen, J. Nizard, Y. Keravel, J. P. Lefaucheur, *Nat. Rev. Neurol.* **7**, 699–709 (2011).
12. J. Cichon, T. J. J. Blanck, W.-B. Gan, G. Yang, *Nat. Neurosci.* **20**, 1122–1132 (2017).
13. M. Jeong *et al*., *Sci. Rep.* **6**, 20072 (2016).
14. R. Muñoz-Castañeda *et al*., *Nature* **598**, 159–166 (2021).
15. X. Wang, X. L. Chou, L. I. Zhang, H. W. Tao, *Trends Neurosci.* **43**, 82–87 (2020).
16. X. Zhang, A. N. van den Pol, *Science* **356**, 853–859 (2017).
17. N. Urbain, M. Deschênes, *Neuron* **56**, 714–725 (2007).
18. C. Kolmac, J. Mitrofanis, *Anat. Embryol.* **199**, 265–280 (1999).
19. V. K. Samineni *et al*., *eNeuro* **4**, ENEURO.0129-16.2017 (2017).
20. J. H. Kim *et al*., *Proc. Natl. Acad. Sci. U.S.A.* **115**, 11078–11083 (2018).
21. L. L. Tan, R. Kuner, *Nat. Rev. Neurosci.* **22**, 458–471 (2021).
22. K. S. Meda *et al*., *Neuron* **102**, 944–959.e3 (2019).
23. Y. Zhu, C. F. Wienecke, G. Nachtrab, X. Chen, *Nature* **530**, 219–222 (2016).
24. T. Huang *et al*., *Nature* **565**, 86–90 (2019).
25. A. François *et al*., *Neuron* **93**, 822–839.e6 (2017).
26. H. C. Moon, Y. S. Park, *J. Pain Res.* **10**, 1125–1134 (2017).
27. C. Soares-Cunha *et al*., *Cell Rep.* **38**, 110380 (2022).
28. A. Andrianarivelo *et al*., *Sci. Adv.* **7**, eabg5970 (2021).
29. N. Schwartz *et al*., *Science* **345**, 535–542 (2014).
30. E. Navratilova, C. W. Atcherley, F. Porreca, *Trends Neurosci.* **38**, 741–750 (2015).

ACKNOWLEDGMENTS

The authors sincerely thank M. Brecht and R.-R. Ji for providing insightful scientific feedback on an earlier version of the manuscript. The authors are grateful to C. Gartner for secretarial assistance, to N. Gehrig, D. Baumgartl-Ahlert, B. Zimmermann, and L. Wang for technical assistance, and D. Mittal for data management. The authors gratefully acknowledge the Interdisciplinary Neurobehavioral Core Facility of Medical Faculty Heidelberg for assistance with behavioral experiments. R.K. is an investigator in the Molecular Medicine Partnership Unit, Heidelberg. **Funding:** This work was funded by the following: German Research Foundation grant in Collaborative Research Center 1158 (to R.K., project B01, B06, Z01; T.K., project B08; A.G., project B10; S.W., project B04). Partial scholarship support was provided from Union Hospital, Tongji Medical college, and Huazhong University of Science and Technology (Z.G.) Partial scholarship support was also provided from China Scholarship Council (H.L.). **Author contributions:** Conceptualization: R.K. Methodology: Z.G., V.G., S.L., M.O., L.L.T., S.W., J.M.C., A.G., T.K. Investigation: Z.G., V.G., S.L., H.L., L.L.T., J.K., C.K., S.W. Visualization: Z.G., S.W., S.L., C.K., M.O. Funding acquisition: R.K., T.K., A.G., S.W. Project administration: R.K., Z.G. Supervision: R.K. Writing – original draft: R.K. Writing – review and editing: Z.G., T.K., S.W., A.G., C.K., M.O., L.L.T., V.G. **Competing interests:** Authors declare that they have no competing interests. **Data and materials availability:** All individual data points are available in the main text or the supplementary materials or stored and curated in public data repository (https://heibox.uni-heidelberg.de/d/c953c55267344092993c/). Code files for analysis of electrophysiological and calcium imaging data are also available at https://heibox.uni-heidelberg.de/d/c953c55267344092993c/.

SUPPLEMENTARY MATERIALS

science.org/doi/10.1126/science.add4391
Materials and Methods
Supplementary note 1
Figs. S1 to S16
Tables S1 to S4
References (*31*–*55*)
MDAR Reproducibility Checklist
Movies S1 to S10

View/request a protocol for this paper from *Bio-protocol*.

Submitted 11 June 2022; accepted 21 November 2022
10.1126/science.add4391